INSTITUTE OF PHYSICS PUBLISHING JOURNAL OF PHYSICS B: ATOMIC, MOLECULAR AND OPTICAL PHYSICS

J. Phys. B: At. Mol. Opt. Phys. **35** (2002) R1–R30 PII: S0953-4075(02)22744-3

TOPICAL REVIEW

Thermionic emission from clusters

J U Andersen, E Bonderup and K Hansen[1]

Institute of Physics and Astronomy, University of Aarhus, DK-8000 Aarhus C, Denmark

Received 1 October 2001, in final form 22 January 2002
Published 27 February 2002
Online at stacks.iop.org/JPhysB/35/R1

Abstract

We discuss the interpretation of delayed electron emission from excited clusters as a statistical process analogous to thermionic emission from a hot filament. We argue that transition state theory is not a good theoretical framework for electron emission. Instead the calculation of emission rates may be based on detailed balance and theoretical or experimental cross sections for electron capture, but there can be large uncertainties in theoretical estimates of cross sections. We emphasize the conceptual simplicity obtained with the introduction of the microcanonical temperature. In experiments, the energy distribution is often so broad that it is essential to account for its modification by depletion, which for a very broad distribution leads to a decay rate inversely proportional to time. Another complication is photon emission, and we present estimates of the radiation intensity based on a simple model of a cluster as a sphere containing a gas of free electrons.

In the analysis of experiments, we first discuss the information about cluster dynamics obtained from studies of photoelectron spectra. However, we focus mainly on a detailed analysis of measurement of the rate of delayed electron emission and its dependence on the cluster excitation. Often the parameters of a statistical description, derived from fits to measurements, have appeared to be inconsistent with estimates from theory or from independent experiments. We analyse a measurement of laser-induced electron emission from small Nb clusters and find that inclusion of anharmonic effects in the heat capacity and, even more important, of the competition by radiative decay leads to more reasonable parameters in the statistical description than obtained from the original analysis. The most detailed studies have been performed for fullerene anions. For most of the measurements, radiative cooling is not significant, but it is important to take into account the finite width of the energy distribution, deriving from the initial heating in an oven. Measured cross sections for electron attachment can be applied in lifetime calculations, and an improved analysis leads to the conclusion that the experiments are consistent with the interpretation of electron emission as thermionic emission.

[1] Present address: Department of Physics, University of Jyväskylä, FIN-40351 Jyväskylä, Finland.

1. Introduction

Delayed electron emission has been established as an important decay channel for excited clusters, both neutral and negatively charged [1]. Typically, the cluster is excited by absorption of one or several photons in the visible or UV range. The initial excitation is then electronic, either a single-electron transition or a plasmon excitation, which couples to single-electron excitations on a femtosecond time scale [2–4]. If the excitation energy exceeds the threshold for electron emission, this may happen on the same time scale by a direct coupling between electronic states [5–7]. Alternatively, the energy may become dispersed over all the degrees of freedom of the system through the coupling between electronic excitations and atomic vibrations, typically on a time scale of picoseconds [2, 6]. Electron emission will then be a much slower, statistical process. The mechanisms for electron emission can be distinguished both by their very different time scales and by the energy spectra of the emitted electrons [6, 7]. We focus in this review on delayed emission on a time scale of tens of nanoseconds or longer.

In the analysis of experiments on delayed electron emission, the crucial question is whether the measurements are consistent with the assumption that all quantum states corresponding to the given excitation energy are populated with the same probability. A full statistical equilibrium includes also states with a free electron, and the detailed balance between emission and absorption processes gives a relation between the emission rate and the cross section for attachment. Comparisons between measurements and statistical calculations have shown very large discrepancies [8, 9] which have been interpreted as evidence for breakdown of the hypothesis of statistical equilibrium. It is the purpose of this review to examine critically both the predictions from statistical theory and the analysis of measurements.

Delayed electron emission has been observed for many different types of molecules and clusters [10, 11], but we consider here only results for the simplest type of cluster, consisting of a single species of atoms. The dynamics of hot isolated clusters is usually dominated by emission of monomers (and/or dimers), electrons and photons. In the macroscopic limit, the level of excitation is specified by a thermodynamic temperature, and the main parameters in the statistical description of the three processes are the evaporation enthalpy, the work function and the emissivity (or absorptivity). Statistical emission of electrons from bulk material is denoted 'thermionic emission', and the rate is given by the Richardson–Dushman formula [12], while the intensity of thermal radiation is given by the blackbody formula, multiplied by an average absorptivity. For an excited cluster the three processes are in competition, and electron emission dominates over evaporation when the atomic binding is much stronger than the electron binding [13]. Partly for this reason, the most detailed studies of delayed electron emission from clusters have been made for refractory metals [8, 14–19] and for fullerenes [7, 9, 20–34].

An important quantity to consider when comparing emission of particles from a cluster to the corresponding process for bulk material is the ratio of the wavelength of the particles to the cluster radius. For an atom with 1 eV kinetic energy the reduced wavelength is a small fraction of an Ångstrom. This implies that we may always picture emitted atoms as localized particles, and there is little difference from evaporation from a bulk surface, except for a difference in dissociation energy. For electrons with typical thermal energies, the reduced wavelength is comparable to the radius of a small cluster, and the quantization of angular momentum can therefore be important for electron emission from clusters. For a 1 eV photon, the reduced wavelength is much larger than the radius of even quite large clusters containing thousands of atoms, and the confinement of the cluster electrons to a volume with an extension small compared with the wavelength of the electromagnetic radiation has a profound influence on the physics of absorption and emission. Strong collective electron oscillations (surface plasmons)

can be excited by the radiation field, which may be considered constant over the cluster, just as for absorption by a single atom (the dipole approximation).

In the description of cluster dynamics there are many interesting and useful analogies to nuclear physics [35–40]. Thus the surface plasmon is analogous to the giant dipole resonance in nuclei, where a collective motion of the protons relative to the neutrons is excited [41,42]. The statistical model is the Bohr compound nucleus [43], with loss of memory of initial conditions and with decay rates determined by statistical factors. As discussed by Bohr and Wheeler [44], the description of the fission process is very similar to the transition state theory of unimolecular chemical reactions, with a potential barrier as a function of a reaction coordinate and with a rate expressed in terms of the number of quantum states at the saddle point of the fission barrier. They also showed that neutron emission can be expressed in the same way, with a barrier equal to the neutron binding energy. The transition state was specified as a neutron moving away from the nucleus just outside the nuclear surface, combined with a quantum state of the residual nucleus. However, they warned that the condition for application of the transition state method, that the reduced wavelength be smaller than the nuclear radius, may not always be fulfilled for neutrons, which are much lighter than fission fragments. Electron emission from clusters is in this respect analogous to neutron emission from nuclei. In a careful discussion of the application of the transition state concept to molecular reactions [45], Wigner listed as a further condition that all systems crossing the potential barrier react. To be emitted or attached, an electron must usually exchange energy with atomic vibrations and, owing to the large mass difference between electrons and atoms, the probability can be quite small for such exchanges. We conclude that, in general, transition state theory is not a good framework for the description. Instead we shall adopt Weisskopf's more general formalism based on detailed balance (or reciprocity). Here, the emission rate is expressed in terms of the cross section for attachment of an electron [46]. This cross section may be estimated theoretically [47], and if both the attachment cross section and the emission rate have been measured, the detailed balance relation can be used to check the assumption of statistical equilibrium.

In a statistical equilibrium, the decay rate is proportional to the ratio of the level densities in the final and initial states, and we apply a thermodynamic description similar to Klots' finite-heat-bath theory [48, 49] to evaluate this ratio. However, we emphasize the use of the microcanonical temperature in the description. As argued in detail in [50], this is the appropriate temperature concept for a small isolated system (see also [46]). For decay of small systems, the temperatures in the initial and final states can be quite different, and the ratio of level densities takes the form of a Boltzmann factor with an effective decay temperature close to the average of the two values. For the distribution in kinetic energy of the emitted electrons, the final temperature is shown to be the appropriate parameter [46].

In an experiment, the emission rate is deduced from the time dependence of the yield. Ideally, this dependence is exponential with a rate constant given by the statistical formula. However, a number of effects may distort this simple picture. We shall mainly discuss two effects which are related to the distribution in internal energy of the clusters: firstly, the distribution can have a substantial width, which can derive either from the production in a source or from a spread in the subsequent excitation. This distribution is then modified by the decay because the clusters with the highest energies have the shortest lifetimes, and if the distribution is broad, the exponential decay is replaced by a yield inversely proportional to time [51]. Secondly, the energy distribution may be modified by photon emission. Blackbody-like spectra of thermal radiation have been observed both for refractory metals [52, 53] and for fullerenes [54], and the quenching of electron emission by radiative cooling has been studied for fullerene anions in a storage ring [55, 56]. Via detailed balance, the intensity of thermal radiation can be estimated from a dielectric description of light absorption by small

particles [57], which has been studied extensively for metal clusters [58, 59]. For fullerenes, the intensity has been calculated from a dielectric model which reproduces the main features of absorption experiments [60], and the calculations reproduce measurements rather well [61].

In the following we first review the theoretical description of thermionic emission. Then we discuss the analysis of experiments and begin with a brief account of measured electron energy spectra [6, 16–19, 23]. The results illustrate clearly the distinction between direct emission and delayed, statistical emission. They also show that, on very short time scales, the competition between the various mechanisms can depend strongly on the method of excitation, for example on the wavelength and duration of a laser pulse [6]. We concentrate on studies of the time dependence of the decay. Among the many measurements on refractory metals we have selected a particularly informative experiment on small Nb clusters for detailed analysis [8]. The original analysis of the measured lifetime versus excitation energy showed large deviations from expectations based on a statistical description, thus indicating perhaps a failure of the assumption of a complete statistical equilibrium [1, 30]. However, an estimate of the intensity of thermal radiation indicates that competition by photon emission could play an important role and, in addition, there may be significant effects of anharmonicity on the vibrational heat capacity.

The other example chosen for detailed analysis is the delayed electron emission from fullerene anions [9, 24–32, 34]. They offer a unique possibility to test the equilibrium hypothesis because both electron capture cross sections and decay rates have been measured. The intensity of thermal photon emission has also been studied in detail for these ions [55, 56, 61]. In most experiments the anions were produced with a fairly large spread in internal energy, and we find that previously reported strong deviations from a statistical description most likely have been caused by insufficient consideration of this aspect. When the finite width of the energy distributions is taken into account, the rate of electron emission after capture by a neutral C_{60} molecule is in excellent agreement with the detailed balance relation and hence confirms the interpretation of the decay as thermionic emission. The rates of emission from the few other fullerene anions studied also appear to be in accord with detailed balance. An experiment on electron emission after laser excitation of cold C_{60}^- ions has very recently confirmed these conclusions [62].

2. Statistical description of electron emission

With the assumption that all states compatible with conservation of energy and angular momentum are populated with equal probability, a simple description is obtained which is known in nuclear physics as Bohr's compound nucleus model [43]. As discussed in the introduction, transition state theory does not seem useful for electron emission from clusters, and instead the formalism developed by Weisskopf for particle emission from nuclei offers a natural framework [46, 47]. The relation between the two descriptions is discussed in the appendix (see also [63, 64]).

2.1. Detailed balance

For particle emission from a cluster in statistical equilibrium, the decay rate is related to the reverse process of particle absorption via detailed balance, i.e. the equality of rates of transitions back and forth between any two quantum states [65]. To obtain rate constants k one sums these transition rates over final states and introduces an appropriate average over initial states. If the number of available states is represented by the level density ρ, the resulting statistical balance may be expressed as

$$k_{decay}\rho_{parent} = k_{formation}\rho_{products}. \tag{1}$$

The role of angular momentum conservation in the process requires special attention (see also the discussions in [46, 66]). For a cluster, most of the angular momentum is usually tied up in collective rotation. The moment of inertia is large and the spacing of rotational energy levels hence very small. Transfer of a significant angular momentum from rotation to internal excitation (vibrational or electronic) is then improbable because excitation of an internal state with large angular momentum must take out a considerable amount of energy from the vibrational heat bath. Thus we may assume the internal and the rotational energy to be separately conserved for an isolated cluster.

Electron attachment or emission leads to only small changes in angular momentum or moment of inertia of a cluster, and the rotational energy is therefore nearly unchanged. Furthermore, the transition probabilities are virtually independent of the rotational state. This may be seen, for example, from an expression for the transition rate as a sum over final states of the square of the matrix element of a transition operator. The function expressing energy conservation should have a finite width corresponding to the reaction time, and owing to the very small spacing of rotational levels one may therefore sum freely over the few final rotational states which give a non-vanishing contribution. Applying closure, one then finds that the rotational quantum numbers disappear from the expression and only an average over the initial orientation of the cluster remains. The rotational degrees of freedom are spectators, and the level densities in equation (1) may be taken to refer to vibrational and electronic states of the cluster only, for fixed internal excitation energy.

On the right-hand side of equation (1), there is a contribution to ρ from the emitted or captured electron, and at first we also specify the energy ϵ of this electron. The level density is then a product of the level density of the daughter and the number of states within a small energy interval $\mathrm{d}\epsilon$ for a free electron, which we imagine to be enclosed in a volume V. The rate of attachment for an electron is equal to its velocity multiplied by its spatial density, V^{-1}, and by the capture cross section, $\sigma_c(\epsilon)$, and from equation (1) one obtains for the rate constant for emission of electrons in the energy interval $\mathrm{d}\epsilon$ [62, 67–71] (see also the appendix),

$$k(E,\epsilon)\,\mathrm{d}\epsilon = \frac{2m}{\pi^2\hbar^3}\sigma_c(\epsilon)\epsilon\frac{\rho_d(E-E_b-\epsilon)}{\rho_p(E)}\,\mathrm{d}\epsilon. \tag{2}$$

Here m is the electron mass and the parent and daughter level densities have indices p and d. The internal excitation energy of the parent is E while E_b is the electron binding. The formula contains an explicit spin degeneracy factor of two for the emitted electron while the electronic degeneracies of the parent and daughter are included in the level densities.

We assume that the electron energy ϵ in equation (2) is a small fraction of the total energy so that $\ln\rho_d(E-E_b-\epsilon)$ may be expanded to first order in ϵ. In this expansion we introduce the microcanonical temperature T_d of the daughter at energy $E-E_b$. A microcanonical ensemble is the ensemble representing a system in statistical equilibrium at well defined energy, and for a system at excitation energy E with level density $\rho(E)$ the microcanonical temperature is defined by

$$\frac{1}{k_B T_m} = \frac{\mathrm{d}}{\mathrm{d}E}\ln\rho(E), \tag{3}$$

where k_B is Boltzmann's constant. The expression in equation (2) now takes the form

$$k(E,\epsilon)\,\mathrm{d}\epsilon = \frac{2m}{\pi^2\hbar^3}\frac{\rho_d(E-E_b)}{\rho_p(E)}\sigma_c(\epsilon)\epsilon\mathrm{e}^{-\epsilon/k_B T_d}\,\mathrm{d}\epsilon, \tag{4}$$

and integrating over ϵ we obtain for the total emission rate constant

$$k(E) = \nu\frac{\rho_d(E-E_b)}{\rho_p(E)}, \tag{5}$$

where

$$\nu \simeq \frac{2mk_B^2}{\pi^2\hbar^3}\sigma_c T_d^2. \tag{6}$$

In the expression for the frequency ν, the cross section is averaged over a thermal energy distribution at the microcanonical temperature T_d,

$$\sigma_c = \int_0^\infty \mathrm{d}\epsilon\, \epsilon \mathrm{e}^{-\epsilon/k_B T_d}\sigma_c(\epsilon) \Big/ \int_0^\infty \mathrm{d}\epsilon\, \epsilon \mathrm{e}^{-\epsilon/k_B T_d}. \tag{7}$$

For a bulk surface, similar arguments based on detailed balance lead to the Richardson–Dushman formula for the rate I_e of electron emission per unit area of a surface at temperature T [12],

$$I_e = \frac{mk_B^2}{2\pi^2\hbar^3}(1-R)T^2 \exp\left(\frac{-W}{k_B T}\right), \tag{8}$$

where W is the work function and R is a reflection coefficient for incident low-energy electrons. This formula corresponds to equations (5) and (6), with the ratio of level densities replaced by a Boltzmann factor, as discussed in section 3, and with $4\sigma_c$ replaced by $(1-R)$ times the unit surface area. In statistical equilibrium, the current of emitted electrons is balanced by the captured fraction, $1-R$, of the inward current. The factor of four is most easily understood for a spherical emitter, for which it may be interpreted as the ratio between the surface area, relevant for emission, and the geometrical cross section for capture.

2.2. Capture cross section

In the description based on detailed balance, the information on the dynamics of the emission process is contained in the capture cross section, $\sigma_c(\epsilon)$, and we discuss simple theoretical estimates which are relevant for the experiments to be analysed. Introducing the angular-momentum quantum number l of the incident electron, we may express the capture cross section as a sum over the corresponding partial cross sections [47, 65],

$$\sigma_c(\epsilon) = \pi\lambda\!\!\!^{-2} \sum_{l=0}^{l_{max}} (2l+1)T(l,\epsilon), \tag{9}$$

where $\lambda\!\!\!^{-}$ is the reduced de Broglie wavelength. As discussed in [65], this expression can be given a pictorial interpretation: the angular momentum $l\hbar$ may be associated with an impact parameter range from $l\lambda\!\!\!^{-}$ to $(l+1)\lambda\!\!\!^{-}$ and the corresponding classical cross section is $\pi\lambda\!\!\!^{-2}(2l+1)$. The transmission factor $T(l,\epsilon)$ can never exceed unity and may be thought of as a sticking probability, and l_{max} is an effective cut-off beyond which this probability is small. For application of a classical model it is required that l_{max} be large. For a first estimate, we may use the geometrical cross section, which for a cluster with N atoms and with a typical atomic volume of 20 Å^3 is of order $\pi r_N^2 \sim 9N^{2/3}$ Å^2. The (classical) l value corresponding to impact parameter r_N decreases with decreasing energy, and it becomes equal to unity at $\epsilon = (e^2/2a_0)(a_0/r_N)^2$, where e is the elementary charge and a_0 the Bohr radius of hydrogen (Gaussian units). Since this energy typically is of the same order as $k_B T_d$, the lowest few angular momenta may dominate the averaged cross section in equation (7) and angular momentum selection rules can therefore be important. With the geometrical cross section and $k_B T_d \sim 0.2$ eV, we obtain from equation (6) a frequency factor ν of order 10^{13}–10^{14} s^{-1} for small clusters, $N < 100$.

The cross section may be enhanced by attraction between the electron and the cluster [47, 72, 73]. The enhancement by the Coulomb force in the formation of a neutral cluster can

easily be evaluated in a classical model. For an electron with impact parameter q, the angular momentum barrier at distance r from the centre of attraction amounts to $\epsilon q^2/r^2$ and adding to this the electrostatic potential $-e^2/r$ from a spherically symmetric charge distribution on the cluster, we obtain the effective potential for the radial motion. We assume that the electron has to get very close to the cluster to lose sufficient energy to get captured into a bound orbit, and the cross section may then be expressed in terms of the impact parameter q_c at which the electron reaches a minimum distance r_N,

$$\pi q_c^2 = \left(1 + \frac{e^2}{r_N \epsilon}\right) \pi r_N^2. \tag{10}$$

The enhancement over the geometrical cross section is typically an order of magnitude. We may then ignore unity in the parentheses and obtain as the condition for a classical description $l_{max} = (2r_N/a_0)^{1/2} > 1$. This condition is energy independent and is always fulfilled. For the averaged cross section in equation (7) we then have

$$\sigma_c \simeq \pi r_N^2 \frac{e^2}{k_B T_d r_N}. \tag{11}$$

A somewhat weaker enhancement is expected for attachment to a neutral cluster due to attraction of the electron by the induced dipole moment [47, 74–76]. The interaction potential is at large distances $-\alpha e^2/2r^4$, where α is the polarizability. The effective potential for the radial motion then has a maximum, and with the asymptotic form of the interaction potential the impact parameter below which the energy exceeds this maximum is given by

$$q_c = (2\alpha e^2/\epsilon)^{1/4}. \tag{12}$$

For $q < q_c$, the electron spirals inwards until it hits the cluster surface. The cross section is then independent of the cluster radius and proportional to $\epsilon^{-1/2}$, and the thermal average in equation (7) becomes the Langevin cross section,

$$\sigma_c = \pi \left(\pi \alpha e^2/(2k_B T_d)\right)^{1/2}. \tag{13}$$

This picture breaks down at high energies where q_c becomes comparable to r_N but this is usually not important for thermal electrons. On the other hand, the classical calculation may not be justified for such electrons since the l value corresponding to the impact parameter in equation (12) is not much larger than unity for $\epsilon \sim k_B T_d$ and $\alpha \sim r_N^3$. However, one obtains nearly the same result from a quantal calculation when the asymptotic condition for small r corresponds to the presence of a sink at $r = 0$ (ingoing-wave approximation) [74].

These cross sections may be strongly reduced due to low sticking probabilities $T(l, \epsilon)$ in equation (9), even for low l values. The electron must lose sufficient energy in the collision to become bound and since it is much lighter than an atom, it may scatter elastically with a large probability. An electron reflected at the cluster surface at energy ϵ' transfers a momentum of order $\hbar k = 2(2m\epsilon')^{1/2}$ to an atom. If the atom is bound in an oscillator with frequency ω, the probability P_{exc} for excitation of the oscillator is then given by the small difference between unity and the absolute square of the expectation value of $\exp(\mathrm{i}kx)$, and for the ground state we obtain

$$P_{exc} \simeq \frac{\epsilon'}{\hbar\omega} \frac{4m}{M}, \tag{14}$$

where M is the atomic mass. This result equals the ratio between the maximum energy transfer to a free atom and the quantum of excitation of the oscillator, $\hbar\omega$. The order of magnitude of the excitation probability is $P_{exc} \sim 10^{-3}$–10^{-4} for $\epsilon' \sim 1$ eV.

The dynamics of attachment or emission of electrons depends also on the availability of bound electron states and, as is well known from atomic spectroscopy [77], charged and neutral

clusters are very different in this respect. For a positive ion, there is an infinite number of Rydberg states in the Coulomb potential, whereas the potential from a neutral atom or cluster may barely accommodate a single bound state. Nevertheless, the existence of such a state may be crucial for the attachment probability near zero energy, as has been suggested for electron attachment to C_{60}, for example [78, 79].

The simple estimate in equation (14) indicates that the cross section can be much smaller than given by equation (11) or (13). However, the interaction of an electron with a cluster is complex; there can be many pathways for excitation, and there is a large uncertainty in theoretical estimates [80–82]. This implies that, contrary to the suggestion in [47], for example, a comparison of observed rates of electron emission with values calculated on the basis of theoretical attachment cross sections does not in general provide a reliable answer to the question whether or not the electron emission is thermionic in character.

3. Microcanonical temperature and finite-heat-bath correction

In equation (3) we have introduced the microcanonical temperature T_m of a system with excitation energy E. This is the appropriate temperature concept even when the clusters emerge from an oven with well defined thermodynamic temperature. Inside the oven, the canonical energy distribution is maintained by rapid energy exchange with gas molecules or with the walls, but outside the oven the clusters are isolated and the energy of individual clusters is the conserved quantity. As suggested by Bohr and Heisenberg, energy and thermodynamic temperature may be regarded as complementary quantities in classical physics, with a relation analogous to Heisenberg's uncertainty relation between position and momentum [83].

In order to evaluate the relation between energy and microcanonical temperature explicitly, it is useful to observe that equation (3) also expresses the relation between the thermodynamic temperature and the most probable energy of a canonical distribution [46, 50]. Owing to a slight skewness of the canonical distribution, there is a small difference between this peak value E at thermodynamic temperature T_m and the average energy, $\bar{E}(T_m)$,

$$E \simeq \bar{E}(T_m) - k_B T_m. \tag{15}$$

The average energy of a canonical distribution is often easy to evaluate, for example for a system of harmonic oscillators. Equation (15) may also be expressed as a relation between the microcanonical and canonical heat capacities, $C_m = C_c - k_B$.

As found in section 2.1 from a Taylor expansion, it is the temperature of the daughter which determines the energy distribution of emitted particles. This was emphasized already by Weisskopf [46]. We obtain a different temperature when we perform a similar Taylor expansion to express the rate constant in equation (5) in Arrhenius form,

$$k(E) = \nu \exp\left(\frac{-E_b}{k_B T_e}\right), \tag{16}$$

with an effective emission temperature T_e. For electron emission, the vibrational level densities of the parent and daughter clusters are very similar, and when a difference in electronic degeneracy is included in ν we may therefore represent the level densities by a single function ρ. When the Taylor expansion of the logarithm of the level density is performed around the midpoint of the energy interval from $E - E_b$ to E, the terms of even order vanish for the ratio in equation (5). Assuming that the heat capacity C_m can be considered constant in the differentiations, we then obtain to fourth order

$$\ln\left(\frac{\rho(E-E_b)}{\rho(E)}\right) \simeq -E_b\frac{\mathrm{d}}{\mathrm{d}E}\ln\rho\,(E-E_b/2) - \frac{1}{24}E_b^3\frac{\mathrm{d}^3}{\mathrm{d}E^3}\ln\rho\,(E-E_b/2)$$
$$\simeq \frac{-E_b}{k_B(T_m-E_b/2C_m)}\left(1+\frac{E_b^2}{12C_m^2(T_m-E_b/2C_m)^2}\right), \tag{17}$$

where T_m is the microcanonical temperature before emission. To second order in $E_b/2C_mT_m$, the emission temperature in equation (16) is therefore given by

$$T_e \simeq T_m - \frac{E_b}{2C_m} - \frac{E_b^2}{12C_m^2T_m}. \tag{18}$$

Related ideas were expressed in Weisskopf's discussion of the statistics of neutron emission from a compound nucleus [46], but instead of introducing an effective decay temperature he chose to keep the initial temperature T_m in equation (16) and introduce an effective binding energy E_b^*. Formulae very similar to equations (16)–(18) are central to Klots' finite-heat-bath theory, and the first-order term in equation (18), equal to half the difference in temperature between parent and daughter, is usually called the finite-heat-bath correction [48, 49]. However, Klots does not introduce the concept of a microcanonical temperature but represents a system with well defined energy by a canonical ensemble with the same decay constant. The 'isokinetic temperature' of this ensemble then corresponds to the emission temperature T_e in equation (16). In our opinion, the above description is conceptually simpler and more transparent.

4. Depletion and $1/t$ law

We now consider an ensemble with energy distribution $g(E,t)$ at time t. The total emission rate $I(t)$ is given in terms of the rate constant $k(E)$ by

$$I(t) = \int \mathrm{d}E\,k(E)g(E,t). \tag{19}$$

Concerning the time dependence of the distribution there is an important distinction between two limiting cases: if the clusters are in contact with a heat reservoir at temperature T, with many energy exchanges on the time scale of the decay, the distribution in energy remains canonical, $g(E,t) \propto \rho(E)\exp(-E/k_BT)$, and the function $g(E,t)$ separates into a product of this canonical energy distribution and a function of time. The emission rate is minus the time derivative of the integrated distribution, and inserting equation (5) with an energy independent factor ν into equation (19) we find that the time dependence is exponential with a rate constant of Arrhenius form (equation (16) with $T_e = T$). This result is so well known that it is often applied also for ensembles of isolated clusters. However, if all interactions with other clusters and with the surroundings can be ignored, including emission and absorption of radiation, the excitation energy E is conserved and the clusters decay individually according to the radioactive decay law with rate constant $k(E)$. The decay then leads to a change in shape of the distribution $g(E,t)$ and the expression for the intensity becomes

$$I(t) = \int \mathrm{d}E\,k(E)g(E,0)\exp(-k(E)t). \tag{20}$$

Exponential decay is now obtained only for a very narrow energy distribution. If the initial distribution is broad compared with the weight function $k(E)\exp(-k(E)t)$, it can be extracted from the integral. The weight function is strongly peaked at an energy corresponding to $k(E) = 1/t$. From a Gaussian approximation to the integrand around the maximum one finds that the peak width varies slowly with time, and hence the integral scales with time

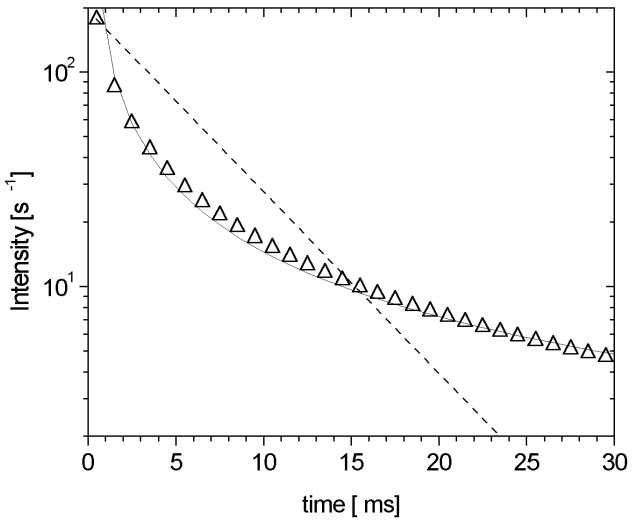

Figure 1. Intensity of electron emission from C_{60}^- ions leaving an oven at 1300 K at $t = 0$. The triangles give the results of a calculation based on equations (16), (18) and (20), with only the first-order finite-heat-bath correction included. The initial distribution in excitation energy of the ions is normalized, and decay parameters are discussed in section 8.2. The solid curve illustrates a $1/t$ dependence and the dashed curve gives the decay rate in thermal equilibrium at 1300 K.

approximately as $1/t$. This argument has often been used in the statistical analysis of experiments, and recently the $1/t$ dependence has been measured directly for clusters and molecules in a storage ring, where the decay can be followed over several orders of magnitude in time [51].

We illustrate the non-exponential decay by a thought experiment. In figure 1 is shown the decay as a function of time of a beam of C_{60}^- ions emerging at $t = 0$ from an oven at temperature $T = 1300$ K. The decay by electron emission was evaluated from equations (16), (18) and (20), with only the first-order finite-heat-bath correction included. The parameters for the rate constant are given in section 8.2, and competing processes like emission of radiation were ignored. The emission rate initially corresponds to decay in thermal equilibrium at 1300 K but its time dependence is very different owing to the rapid depletion of the high-energy tail of the distribution, which dominates the decay in thermal equilibrium. This depletion is sometimes referred to as evaporative cooling[2]. The time dependence of the decay is much closer to the $1/t$ law obtained for a very broad energy distribution. This law does not contain any characteristic time and the apparent lifetime derived from observation within a narrow time window can therefore be determined more by this time window than by the physical parameters of the decay. On the other hand, the $1/t$ dependence can be a useful reference [51], for example for the measurements of radiative cooling discussed below.

5. Photon emission

For small clusters, emission of a single photon usually gives a large change in the lifetime for electron emission, and we may treat electromagnetic radiation as an alternative decay

[2] In our opinion, the term 'evaporative cooling' should only be used for an ensemble of interacting systems, where the high-energy tail is continuously repopulated. An example is cooling of individual clusters by successive dissociation of monomers.

channel. For large clusters, on the other hand, radiation can be treated as a continuous cooling mechanism, which gradually quenches electron emission. Often it can be difficult to detect the influence of radiation directly and one must rely on theoretical estimates. We shall derive a simple estimate of the radiation intensity, based again on detailed balance.

5.1. Radiation from an isolated cluster

We wish to express the rate of spontaneous emission in terms of the cross section for absorption. To this end we first apply the detailed balance, as given by equation (1), to relate the Einstein coefficient $B_e(E,\omega)$ for induced emission at frequency ω from a cluster at excitation energy E to the absorption cross section $\sigma_{abs}(E-\hbar\omega,\omega)$ at the lower energy $E-\hbar\omega$,

$$\hbar\omega B_e(E,\omega) = c\sigma_{abs}(E-\hbar\omega,\omega)\rho(E-\hbar\omega)/\rho(E). \tag{21}$$

Here, c is the speed of light and the densities of states $\rho(E-\hbar\omega)$ and $\rho(E)$ account for the degeneracy of the levels at energies $E-\hbar\omega$ and E. To obtain the intensity of spontaneous emission, we multiply the expression in equation (21) by the ratio between A and B_e coefficients. This ratio equals the energy per unit volume and unit frequency interval when each mode in the radiation field is occupied by a single photon, i.e. $A/B_e = \hbar\omega^3/(\pi^2c^3)$. We therefore obtain for the radiation power per unit frequency interval,

$$I_r(E,\omega) = \frac{\hbar\omega^3}{\pi^2c^2}\sigma_{abs}(E-\hbar\omega,\omega)\frac{\rho(E-\hbar\omega)}{\rho(E)}. \tag{22}$$

In an absorption experiment, one does not determine σ_{abs} but rather an effective cross section σ, which is reduced owing to induced emission. Even more important, this cross section is the quantity which fulfils sum rules independent of the initial excitation energy $E-\hbar\omega$; for transitions between harmonic oscillator levels, for example in absorption of infrared radiation by vibrations, it is even completely independent of the initial energy. It is therefore for σ rather than for σ_{abs} that we shall derive an expression from a simple model. Applying detailed balance once again, we obtain for the relation between the effective cross section and the absorption cross section,

$$\sigma(E-\hbar\omega,\omega) = \sigma_{abs}(E-\hbar\omega,\omega) - \sigma_{abs}(E-2\hbar\omega,\omega)\rho(E-2\hbar\omega)/\rho(E-\hbar\omega). \tag{23}$$

For an ensemble described by a canonical distribution with a population proportional to $\rho(E)\exp(-E/k_BT)$ integration over E leads to a very simple connection between the two cross sections,

$$\sigma_{abs}(T,\omega) = \sigma(T,\omega)\frac{1}{1-\mathrm{e}^{-\hbar\omega/k_BT}}. \tag{24}$$

Applying this relation, we find for the corresponding average of the expression in equation (22) [60],

$$I_r(T,\omega) = \frac{\hbar\omega^3}{\pi^2c^2}\sigma(T,\omega)\frac{1}{\exp(\hbar\omega/k_BT)-1}. \tag{25}$$

The difference between the Boltzmann factor and the Planck factor is important for photon energies of the order of k_BT or smaller.

We now return to the microcanonical ensemble relevant for isolated clusters. In the expression for the radiation intensity in equation (22) we may approximate the ratio of level densities by a Boltzmann factor, as discussed in section 3, and to first order we obtain the emission temperature $T_m - \hbar\omega/2C_m$. We want again to introduce the effective cross section σ. Since the difference between the two cross sections is important only for very small photon energies, we may in the last term in equation (23) increase the energy argument by $\hbar\omega$ in the

cross section and expand the logarithm of the ratio of level densities around the value $E-\hbar\omega/2$ as before. This leads to an expression analogous to equation (25),

$$I_r(E,\omega) \simeq \frac{\hbar\omega^3}{\pi^2c^2}\sigma(E-\hbar\omega,\omega)\frac{1}{\exp(\hbar\omega/k_B(T_m-\hbar\omega/2C_m))-1}. \tag{26}$$

5.2. Dielectric model

For clusters decaying by thermionic emission on a micro- to millisecond time scale, the temperature is so high that the radiation is usually dominated by electronic transitions. Most of the oscillator strength resides in collective oscillations of electrons, and we shall represent these by a simple dielectric model. A century ago, Mie solved the problem of the scattering and absorption of electromagnetic radiation by a spherical object described by a dielectric function $\epsilon(\omega)$ [57]. The general formulae are quite complicated but they simplify when the radius of the sphere is small compared with the reduced wavelength c/ω of the radiation. In this limit, which is of interest here, the formulae may also be derived in a much simpler way [57 (section 5.2), 60]. For a sphere of radius r_N one obtains the absorption cross section

$$\sigma(\omega) = \pi r_N^2\frac{4\omega r_N}{c}\mathrm{Im}\,\frac{\epsilon(\omega)-1}{\epsilon(\omega)+2}, \tag{27}$$

and this expression, which fulfils the sum rules [60], will be applied in equation (26). In estimates of the radiation from clusters, based on Mie's theory, the last factor in equation (27) has often been assumed to be close to unity (see, for example, [15, equation (B1)]). We evaluate this factor for a simple dielectric function, pertaining to a free electron gas,

$$\epsilon(\omega) = 1-\frac{\omega_p^2}{\omega(\omega+\mathrm{i}\gamma)}. \tag{28}$$

Here ω_p is the plasma frequency, related to the density n of valence electrons through $\omega_p^2 = 4\pi e^2 n/m$, and γ is a damping constant. Inserted into equation (27), this dielectric function leads to a surface plasmon resonance at the frequency $\omega_p/\sqrt{3}$ with a width determined by γ. At the temperatures of interest, up to several thousand degrees, the power emitted is normally dominated by much lower frequencies at which the imaginary part in equation (27) may be replaced by its low-frequency limit. A combination of equations (27) and (28) then yields

$$\sigma(\omega) \simeq \pi r_N^2\frac{4\omega r_N}{c}\frac{3\gamma\omega}{\omega_p^2}. \tag{29}$$

We now insert this formula into equation (26) and integrate over frequencies. The result is expressed as the blackbody formula with geometrical surface area and an effective absorptivity (or emissivity) $a(T)$,

$$I_r = 4\pi r_N^2\sigma_0 a(T_m)T_m^4, \tag{30}$$

where the Stefan–Boltzmann constant σ_0 equals $\pi^2k_B^4/(60c^2\hbar^3)$ and has the value 3.54×10^{-9} eV s^{-1} Å^{-2} K^{-4}. The absorptivity is given by

$$a(T) = 12\frac{\gamma r_N}{c}\frac{\langle\omega^2\rangle}{\omega_p^2}, \tag{31}$$

where the brackets indicate an average over the Planck distribution, with a finite-heat-bath correction

$$\langle\omega^2\rangle = \frac{\hbar^4}{(k_BT)^4}\frac{15}{\pi^4}\int_0^\infty\frac{\mathrm{d}\omega\,\omega^5}{\exp\left[\hbar\omega/(k_BT-\hbar\omega k_B/2C_m)\right]-1}. \tag{32}$$

This expression is proportional to T^2, and in the limit $k_B/C_m \rightarrow 0$ we have $\langle(\hbar\omega)^2\rangle \simeq 19(k_BT)^2$. A simple estimate of the plasmon width, which appears often to be reasonable for small metal particles [58,59], is $\gamma = \xi v_F/r_N$ with $\xi \sim 0.5$–1, where v_F is the Fermi velocity of the valence electrons and is of the order of the Bohr velocity $c/137$. For large clusters, γ may instead be estimated from measurements of electron energy loss in bulk material.

The intensities predicted from these formulae are typically an order of magnitude lower than the values obtained from equation (27) with the last factor equal to unity. Furthermore, the spectral shape is modified by an additional factor ω in equation (29) and, as a consequence, the dependence of the total intensity on temperature is changed from the fifth to the sixth power of T. The distribution in wavelength has been measured for C_{60} [54] and for large metal clusters [52,53], and the temperatures were determined from fits with a spectral function that did not include the additional factor ω. The temperatures derived with the modified function are lower by 10–15%.

5.3. Measurements of radiation from clusters

The cooling rate of large clusters can be determined from measurements of the radiation spectrum as a function of time, as demonstrated in [53] for very large Nb clusters ($N \sim 13\,000$). This measurement is here of special interest because we shall later analyse measurements of the rate of electron emission from small Nb clusters, which could be influenced by photon emission. The measured cooling rates are factors of 2–4 higher than obtained from our estimate with $\hbar\omega_p = 20$ eV and $\hbar\gamma = 10$ eV [84] and with heat capacity $3Nk_B$. However, as noted by the authors, the temperatures $T \gtrsim 3000$ K are so high that also emission of particles may contribute to the cooling.

The most precise information about cluster cooling rates has been obtained for fullerenes from the type of results illustrated in figure 2 [61]. The C_{56}^- ions were injected into a storage ring from a plasma source, with an initial distribution in excitation energy even broader than for the thought experiment illustrated in figure 1. Hence the decay should follow the $1/t$ dependence given by the dashed line. However, the electron emission is quenched by radiative cooling for times longer than $\tau_c \sim 1$ ms, and from the measured value of this time the radiation intensity can be deduced [55,61]. For fullerenes, the heat capacity is so large that the quenching typically requires emission of several photons, and the effect of the heat radiation may to a good approximation be modelled as a continuous cooling. The intensity has been calculated from a dielectric model, with parameters adjusted to account for the main features of the absorption spectrum, and the result is reproduced by the type of estimate given above [60]. The predictions are in good agreement with measurements of the quenching of particle emission, both for electrons at temperatures $T \lesssim 1500$ K [61] and for C_2 at much higher temperatures, $T \gtrsim 3000$ K [85,86].

Measurements in a storage ring have also been carried out for electron emission from anions of small metal clusters [51], and an example is shown in figure 3. The following analysis of this measurement may serve as an illustration of the application of the formalism developed in the previous sections: the Al_7^- ions were created in a sputter ion source with a broad distribution in excitation energy. In contrast to the fullerenes, the Al_7^- clusters are so small that typically emission of a single photon is sufficient to quench the electron emission, and radiation may therefore be included as a competitive decay channel. For photons, the emission rate varies much more slowly with temperature than for electrons and we may therefore approximate this rate by a constant $1/\tau$ which is added to $k(E)$ in the exponent in equation (20). The integral then gives a time dependence proportional to $\exp(-t/\tau)/t$, and this function is seen to fit the measurements for $\tau = 2.3$ ms. To demonstrate that the time

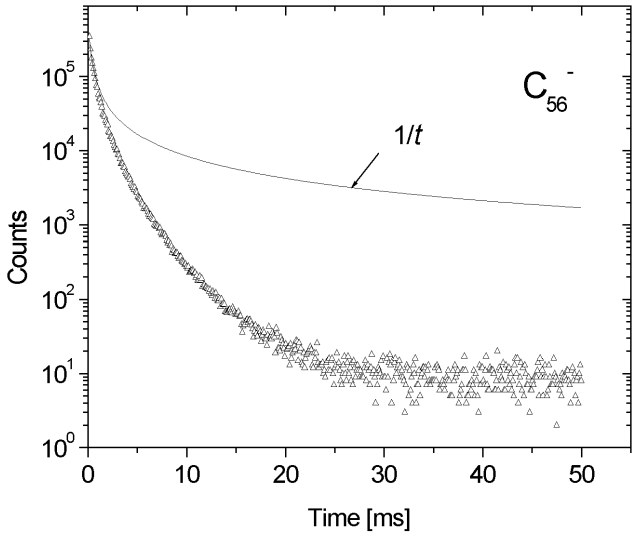

Figure 2. Observation of electron emission from C_{56}^- ions in the storage ring ELISA (from [61]). The ions were produced in a hot plasma source and without photon emission the yield should be inversely proportional to time. Hence the reduction relative to the curve labelled $1/t$ gives the quenching of thermionic emission by radiative cooling.

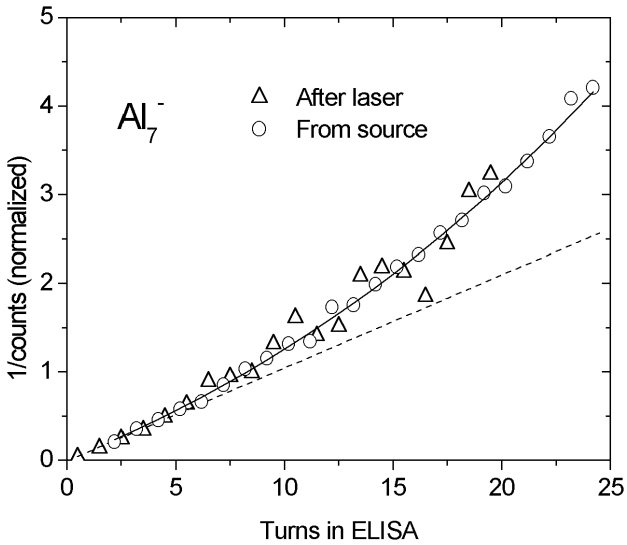

Figure 3. The reciprocal of the counts of neutrals (o), recorded turn by turn after injection of Al_7^- clusters from a sputter source into the storage ring ELISA (from [51]). One turn corresponds to about 50 μs. The triangles indicate the reciprocal counts after excitation of the stored clusters with a laser pulse. The curves show reciprocal yields proportional to time t (dashed) and to $t\exp(t/\tau)$, with $\tau = 2.3$ ms.

dependence is characteristic for the statistical ensemble and does not depend on the means of excitation, the decay was also recorded after re-excitation with a laser pulse after about 20 ms. The results after a renormalization are given by the triangles in figure 3.

In order to compare with the radiation intensity given by equations (30)–(32), we first estimate the cluster temperature at $t \sim 2$ ms from the formulae for electron emission. Choosing $\nu = 10^{11}$ s^{-1} as a first guess, we obtain an effective decay temperature of $T_e \simeq 1180$ K from equation (16) with $E_b = 1.9$ eV [87]. According to equation (18), this gives $T_m \simeq 2060$ K and $T_d \simeq 490$ K for a heat capacity of $C_m = 14k_B$. We can now check whether our guess for the magnitude of ν was reasonable. From equations (6) and (13) we obtain $\nu = 3.7 \times 10^{12}$ s^{-1}, so our choice corresponds to a sticking probability in the range 10^{-1}–10^{-2}. This is an acceptable value and a change of ν by a factor of ten does not modify the result much. To estimate the rate of photon emission, we remove a factor $\hbar\omega$ from equation (26) before integration, and obtain the expression in equations (30) and (31) with a factor $\hbar\omega$ removed from the integral in equation (32). The bulk plasma frequency is 17 eV for Al, and the simple estimate for the width, $\gamma \simeq v_F/r_N$, gives $\hbar\gamma \simeq 5$ eV. We then obtain a rate of about 0.5×10^3 s^{-1}, in excellent agreement with the measured lifetime. Measurements for the neighbouring clusters, with $N = 8$ and 9, gave very similar radiation lifetimes τ.

6. Energy distribution of emitted electrons

In addition to a time delay, thermionic emission from clusters is characterized by a thermal kinetic energy distribution, as expressed in equation (4). We shall briefly review the information about the dynamics of electron emission that has been gained from studies of electron spectra from photo-excited clusters. A number of experiments, with increasing sophistication in measurement and analysis, have been made on the emission from small W_N^- clusters after absorption of a single photon [13, 16, 17, 19]. Spectra for $N = 4$–11 from [19] are shown in figure 4. The electrons were emitted within the first 0.1–1 μs after absorption of a 4.0 eV photon, and the spectra clearly contain two components, a low-energy part and structures at higher energy, which presumably stem from direct processes. The curves are fits to the low-energy part and are proportional to a Boltzmann factor $\exp(-\epsilon/k_BT)$ times ϵ for the dashed curves and $\sqrt{\epsilon}$ for the full drawn curves. Clearly, the latter curves give the better fits, as expected from equation (4) and the cross section πq_c^2 obtained from equation (12). In the earlier papers [13, 16] the resolution at the lowest energies was poor, and the spectra were simply fitted with a Boltzmann distribution.

The temperatures used in the fits are given in the figure. They correspond to the effective decay temperature T_e in equation (18) with a first-order finite-heat-bath correction. However, according to our discussion in section 2.1, the temperature governing the shape of the electron spectrum should be the daughter temperature T_d, which is lower by about 25%. The width of the calculated curves should be reduced by this amount. It is perhaps not so surprising that the spectra are broader than expected for emission in a full statistical equilibrium since the measurements include electrons emitted at very short times [7]; it would be interesting to have spectra recorded with a delay after the photon absorption. In the earlier papers, the error in the temperature was about twice as large since it was estimated as the photon energy divided by the heat capacity [13, 16, 17]. However, this is not important for the qualitative distinction between direct and statistical processes, which was used to establish a correlation between the observation of thermal electrons and the relative magnitude of the electron affinity and the heat of vaporization in bulk material [13].

Very detailed investigations of the dependence of the photoelectron spectra on the mode of excitation have been carried out for the 'magic' molecule C_{60} with ionization energy 7.6 eV. Delayed ionization from neutral C_{60}, interpreted as thermionic emission, was first observed in [21, 22]. In [23] it was shown that the peaks corresponding to direct multi-photon ionization

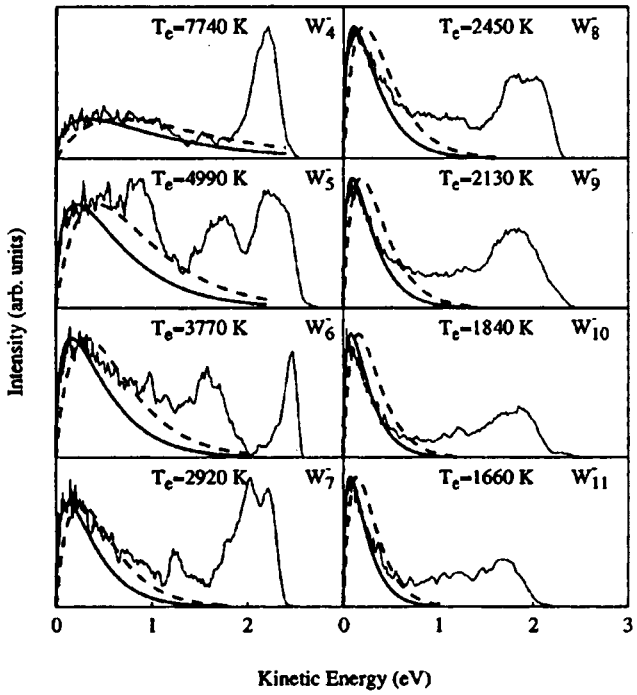

Figure 4. Kinetic energy spectra of electrons emitted from tungsten cluster anions within 0.1–1 μs after excitation by photon absorption (from [19]). The fits to the low-energy part of the spectra are discussed in the text.

disappeared when a delay was introduced in the electron detection. For laser wavelengths above 200 nm the energy spectrum was dominated by low-energy electrons, and it was in good agreement with a Boltzmann distribution (equations (4) and (10) with a reasonable daughter temperature T_d). Other measurements have shown that the delayed ionization disappears for laser wavelengths below 213 nm [88], and this can be understood as a depletion of the hot clusters by single-photon ionization out of the excited triplet states with $\sim$1.7 eV excitation energy [89]. The recent study in [6] is very informative about the processes involved in the redistribution of an initial electronic excitation on other degrees of freedom. With ultrashort pulses from a 790 nm laser, coherent multi-photon ionization was observed for pulse lengths less than 100 fs (above-threshold ionization); in the range 100 fs to 1 ps there was evidence for statistical redistribution of the energy among the electronic degrees of freedom, only (see also [5,7]), and finally for pulse lengths longer than 1 ps there appeared to be statistical emission after coupling between the electronic and vibrational degrees of freedom.

7. Rates of delayed electron emission from small Nb clusters

We now turn to the central subject of this review, an analysis of experiments on decay rates for delayed electron emission from clusters. As our first example, we take the measurements by Collings *et al* on neutral Nb_N clusters, with $5 \leqslant N \leqslant 13$, excited by absorption of 2–4 photons, each with an energy of 3–4 eV [8]. The photon energies were so high that only one particular number of absorbed photons gave rise to emission on the time scale of the measurement ($\sim$1 μs). The internal energy of the clusters before absorption corresponded to

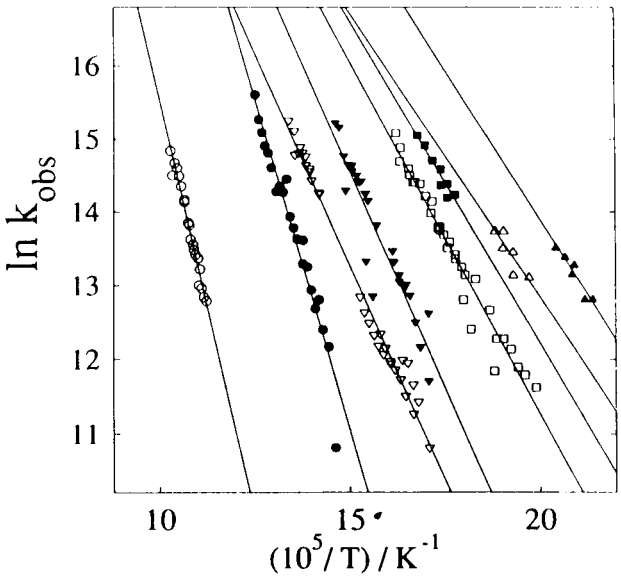

Figure 5. Arrhenius-like plots for thermionic emission from multi-photon excited Nb_N clusters (from [8]). The logarithm of the rate constant k (s^{-1}) is plotted against the reciprocal internal microcanonical temperature before emission, and from left to right the data correspond to $N = 5, 6, 7, 8, 9, 11, 12$ and 13. The lines are linear fits.

temperatures of 300–600 K and was in all cases only a small fraction of the total excitation energy. Hence the energy distributions may be approximated by δ-functions and the decay should be exponential; this was confirmed by the measurements [14]. The interpretation of the electron emission as statistical or 'thermionic' emission was supported by the observation that a change of the excitation energy by a variation in photon wavelength produced the same change in lifetime as a change through a variation of the initial temperature.

As shown in figure 5, the data in [8] were presented in an Arrhenius plot of $\ln k$ versus $1/T$, with a value of T equal to the microcanonical temperature T_m at the initial excitation. A heat capacity derived from a harmonic oscillator model for the cluster vibrations was used. The statistical analysis of the data was based on Klots' finite-heat-bath theory [48, 49]. We have instead fitted the expressions in equations (5) and (17) to the data. Since the reverse process is attachment to an ion, we have assumed ν to be proportional to the temperature of the cluster after the emission, as obtained from equations (6) and (11). With this temperature dependence of ν, the expression in equation (5) is equivalent to the formula from transition-state theory which was the starting point for the original analysis, and we can compare directly with the parameters derived in [8] (see appendix). We have obtained the parameters E_b and ν from a match to the straight lines through the data, and we have checked that over the range of the measurements the expression in equation (17) is indeed close to a straight line in such a plot and that the error on E_b introduced by the expansion is very small ($\sim$1%). For the microcanonical heat capacity in equation (17) we have used the high-temperature limit for harmonic vibrations, $C_m = (3N - 7)k_B$. We have checked that the values of T corresponding to the data points in figure 5 are reproduced quite accurately with this approximation.

In figure 6 our results for the energy barrier E_b are compared with the values obtained in [8]. The overall agreement is rather good but there are significant differences. We find the barrier to be lower for $N = 7$ than for the neighbouring clusters, and it is surprising that this structure is absent in the original analysis because it is clearly visible in the data in figure 5.

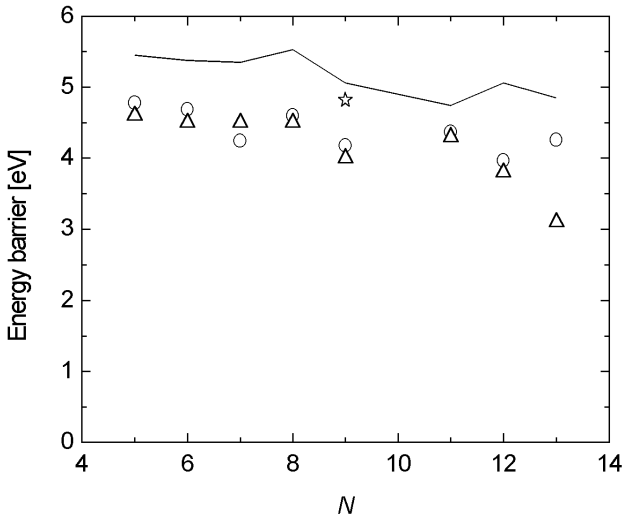

Figure 6. Energy barriers for electron emission from Nb_N clusters, derived from the measurements illustrated in figure 5. The circles give the binding energies E_b derived from fits of equations (5) and (17) to the lines in figure 5, while the triangles represent the values in table II of [8]. The solid curve connects the ionization potentials from the same table. Reference [38] lists measured values for the work function of solid Nb in the range 4–4.9 eV. The star indicates the result obtained from an analysis including the competition from photon emission.

The largest discrepancy occurs for $N = 13$ where a very low value of E_b was found in [8] while our value is similar to those for the other clusters. This difference is important for the qualitative conclusions drawn from the analysis [1]. The energy barriers derived are on average lower than the ionization potentials by ∼0.8 eV, i.e. by about 15%. As discussed by Collings *et al*, the energy barrier may be lower than the ionization energy due to atomic relaxation. Also, the clusters are very hot even after electron emission, and the ionization potentials have been measured at much lower temperature. Still, the deviations seem rather large. An even more serious deviation from the parameters expected for statistical emission is the value of the pre-exponential frequency factor. We find from our analysis $\nu \sim 10^{11}\ s^{-1}$, in good accord with [8]. This value is much lower than the estimate, $\nu \sim 10^{15}\ s^{-1}$, obtained from equations (6) and (11). As discussed in section 2.2, it is conceivable that the cross section for attachment could be strongly reduced if there is no efficient channel for energy transfer from an incident electron, but four orders of magnitude is a very large reduction.

We have examined other possible explanations for the low value of ν (see also the discussions in [8, 30]). The heat capacity applied corresponds to harmonic vibrations and for the very high temperatures reached in the experiment, close to 10^4 K for the smallest clusters, there may be significant anharmonic effects. In fact, the heat capacity for solid niobium increases strongly from the Dulong–Petit value for temperatures approaching the melting point near 2700 K [90]. In addition, the heat of melting corresponds to a heating by about 1000 K [91]. To estimate the influence on our analysis, we have multiplied the heat capacity by a factor $(1 + T[\mathrm{K}]/10^4)$. We have reduced the temperatures in figure 5 by the corresponding relation $T[K] \rightarrow 10^4(-1 + (1 + 2 \times 10^{-4} T[\mathrm{K}])^{1/2})$ and have also applied the new relation between energy and temperature in the evaluation of the two derivatives in equation (17). As it turns out, this leaves the electron binding energies obtained from the fits virtually unchanged but the pre-exponential factors are increased by an order of magnitude!

Another important effect is the decay by emission of photons. As an example, we have examined the consequences of a significant competition by radiative decay for the average-size cluster in the experiment, $N = 9$, for which the data cover nearly two orders of magnitude in the measured lifetime (figure 5). As in our analysis of the decay of Al_7^- clusters (figure 3), we assume that emission of a single photon is sufficient to quench the decay. The cluster radius is $r_N \simeq 3$ Å, and as before we take the bulk plasmon resonance to be at $\hbar\omega_p = 20$ eV with a width $\hbar\gamma = 10$ eV [84]. At a temperature of $T = 5 \times 10^3$ K we then obtain from equations (30)–(32) a rate of photon emission, $\sim 10^5$ s^{-1}, which is of the same order as the lowest measured rates of electron emission in figure 5. We have included a photon emission rate proportional to T^5 and also the linear increase of the heat capacity with temperature discussed above. Adjusting as before the parameters E_b and ν to fit the straight line through the data in the Arrhenius plot in figure 5, we find E_b to be increased by 0.64 eV and ν to be increased by a factor of 70 relative to the values derived in the first analysis. The fit is now not quite a straight line but has a positive curvature at the lowest temperatures. There may be an indication of such a curvature in the data for $N = 7$ and 9 but it is within the scatter of the data.

We conclude that when the analysis includes a temperature dependence of the heat capacity similar to bulk values and a competition by radiative decay, we obtain a much better agreement with predictions. The electron binding is now quite close to the measured ionization potential (figure 6). The value of the pre-exponential factor is still quite small compared with the estimate from detailed balance with the capture cross section given by equation (11), but the reduction is now of a magnitude which could be explained by sticking probabilities of order 10^{-2}.

8. Formation and decay of fullerene anions

The fullerenes, and in particular C_{60} and C_{70}, have a special position in this picture. The electron affinity is known for most fullerenes [92] and, as discussed in section 5.3, the influence of radiative decay on electron emission has been studied in detail. Cooling turns out not to be important on a time scale much shorter than a millisecond (see figure 2). The loss of atoms is dominated by C_2 emission, and the energy barrier is so high that this channel is completely suppressed in anions. Furthermore, both emission rates and cross sections for electron attachment have been measured, and this allows a test of the assumption of a statistical equilibrium in the decaying anions.

Energy-resolved capture cross sections have been measured with crossed beams of electrons and fullerene molecules from an oven [24, 26–29, 32, 34]. It is difficult to determine absolute cross sections but from one experiment values between 20 and 80 Å^2 were reported, with a strong resonance a little above zero energy ($\epsilon \sim 0.2$ eV) [29]. The magnitude is close to the geometrical cross section, $\sigma_c \simeq 50$ Å^2 for a radius of $\sim$4 Å. In this and in the other early crossed-beam experiments, there seemed to be a strong decrease of the cross section at zero energy and this was interpreted as absence of s-wave attachment [93]. These observations agreed with flowing-afterglow experiments (FALP), which yield absolute cross sections of 80–100 Å^2 at electron temperatures of a few thousand K but a much lower attachment rate at low electron temperatures [25, 31].

Since the energies of thermally emitted electrons are typically a few tenths of an eV only, the behaviour of the capture cross section near zero energy is important for calculation of emission rates via detailed balance. There was already some early evidence against the suggested absence of s-wave attachment: significant capture rates were measured in collisions between atoms in a high Rydberg state and C_{60} and C_{70} molecules [78, 79], and this strongly indicated that there should be a finite attachment cross section at very low electron energies and, consequently, a finite contribution from s-wave capture. Furthermore, a new analysis

of data from one of the crossed-beam experiments also indicated the presence of an s-wave contribution [79]. Despite the difficulty in performing crossed-beam experiments at very low electron energies, the recent measurements in [32, 34] seem now to have established the presence of a quite strong s-wave contribution to the capture of low-energy electrons by C_{60}. At the same time, more sophisticated theoretical calculations [94] indicate that the estimates in [93] were too crude to be reliable. However, the physical mechanism of the s-wave capture is not yet clear. An interesting suggestion is capture via a real or virtual bound state in the polarization potential [78, 79, 94]. There is also an unresolved discrepancy with the FALP measurements. The internal temperature of the molecules could be important since the coupling between electronic and vibrational excitations increases strongly with temperature. Due to gas cooling in the FALP measurements, the internal temperature of the fullerene molecules was lower than in the crossed-beam experiments, where the molecules exit an oven at $T \sim 800$ K.

Although the absolute magnitude of the cross section at low electron energies is still somewhat uncertain, there is sufficient information for an approximate calculation of emission rates, based on detailed balance as discussed in section 2. In the following we shall apply values of $\sigma_c = 20$ and 60 Å^2 as alternatives to represent the likely range of the thermally averaged attachment cross section for C_{60}. These values are an order of magnitude smaller than the Langevin cross section in equation (13), which with the polarizability of 82 Å^3 for C_{60} becomes $\sigma_c \simeq 350$ Å^2 for $k_B T_d = 0.15$ eV.

8.1. Early studies of electron emission from C_{60}^-

Delayed electron emission from fullerene anions was first observed by Smalley's group [20]. Subsequently the process was studied in detail by Yeretzian *et al* with the aim to establish whether it could be understood as thermionic emission [9]. In these experiments, the internal energy was varied through a change of the collision energy in reflection of the ions from a Si surface, and the logarithm of the measured decay rate was found to be approximately linear in the reciprocal perpendicular collision energy, as illustrated in figure 3 of [9]. On the assumption that the average energy converted into molecular excitation in the reflection is proportional to the collision energy, this figure can be interpreted as an Arrhenius plot. The value of the proportionality constant could be adjusted to give agreement between the apparent activation energy and the electron affinity, but the intercept with the ordinate axis was at a much lower frequency, $\nu \simeq 10^8$ s^{-1}, than expected from a statistical calculation. It was therefore concluded that the results were incompatible with the equilibrium hypothesis. We shall argue that this conclusion is probably not correct.

To understand the results we must consider the analysis of the experiment in some detail. At each collision energy, an ensemble of molecules was created with a considerable spread in excitation energy, and the observed time dependence of the emission intensity could not be described by a single exponential. One therefore considered the average rate constant, which according to equation (20) is equal to the initial value of the electron intensity from a normalized distribution, $\bar{k} = I(0)$. In figure 7, the data points from [9] represent the normalized decay rate at short times, and they are here plotted at energies E equal to 16% of the perpendicular kinetic energy of the molecules before reflection from the Si surface. The lines represent our calculations. We have used the rate constant $k(E)$ in equation (16) with the parameters discussed below in the analysis of the crossed-beam experiments, and this function is given by the dashed curve. The three solid curves give the average rate constant for energy distributions that are 2, 3 and 4 times wider than a canonical distribution, which has an rms width of about 10%, and the logarithmic slope is seen to decrease strongly with increasing width. Our calculations also contain a correction for the finite time resolution $\delta t \sim 0.1$ μs of

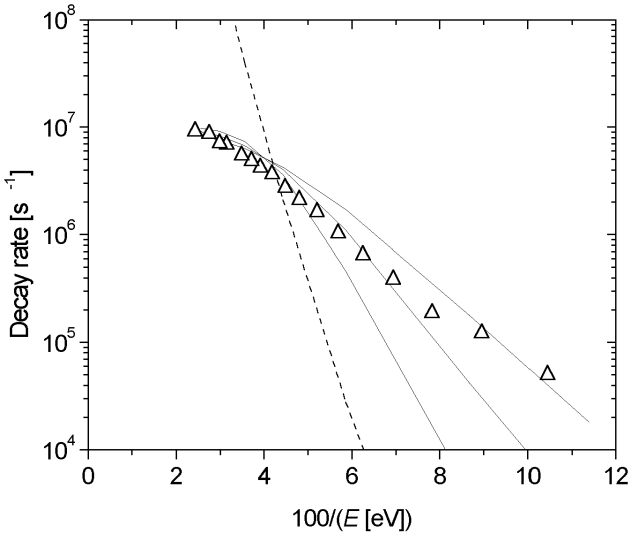

Figure 7. Analysis of the decay rates for C_{60}^- ions reflected from a solid surface with average excitation energy E [9]. The dashed curve gives the rate constant, as in figure 9 below. The solid curves are calculated from equation (33) for $\delta t = 0.1\,\mu$s and for Gaussian energy distributions with 2, 3 and 4 times the canonical width, which is about $\pm 10\%$. The data points are from [9].

the experiment: the quantity derived from the measurements is not $I(0)$ but the intensity $I(t)$ averaged over the interval from 0 to δt, and from equation (20) we obtain

$$\bar{k}_{exp} \simeq \frac{1}{\delta t}\int_0^{\delta t} \mathrm{d}t\, I(t) = \frac{1}{\delta t}\int_0^{\infty} \mathrm{d}E\, g(E,0)(1-\exp(-k(E)\delta t)), \tag{33}$$

where the function $g(E,0)$ represents the distribution in excitation energy just after the surface collision at $t = 0$. At high collision energies, the exponential term can be neglected and the equation leads to a limiting value, $\bar{k}_{exp} \to \delta t^{-1}$. Indeed, such a saturation is observed in the data in figure 7. A different analysis was attempted in [9] for the measurements at the highest energies and this gave slightly higher values of $\bar{k}_{exp}$, but it is simply not possible to extract information about frequencies higher than $\sim\delta t^{-1}$ from data recorded with time resolution δt.

We may conclude that the apparent large discrepancy between the results of this experiment and a statistical picture of electron emission is strongly reduced when reasonable estimates of the width of the energy distributions and of the experimental time resolution are included in the analysis. In [95] it was suggested that the molecules could have an additional high excitation energy from the initial laser desorption process, but they should be cooled efficiently by the carrier gas in the type of source used in the experiment. A similar source in the same laboratory produced large sodium clusters without shell structure from evaporation in the mass spectrum. The stability of these clusters gives an upper limit of less than 400 K for $N > 100$ [96].

8.2. Delayed electron emission from C_{60}^- after electron attachment

Measurements of the lifetime as a function of excitation energy have been performed in conjunction with crossed-beam attachment experiments [26,32,34]. Here the excitation energy can be calculated fairly accurately, and the experiments have yielded consistent lifetimes which differ substantially from those obtained in the earlier measurements. The connection between decay rate and attachment cross section has been discussed by Matejcik *et al* who considered

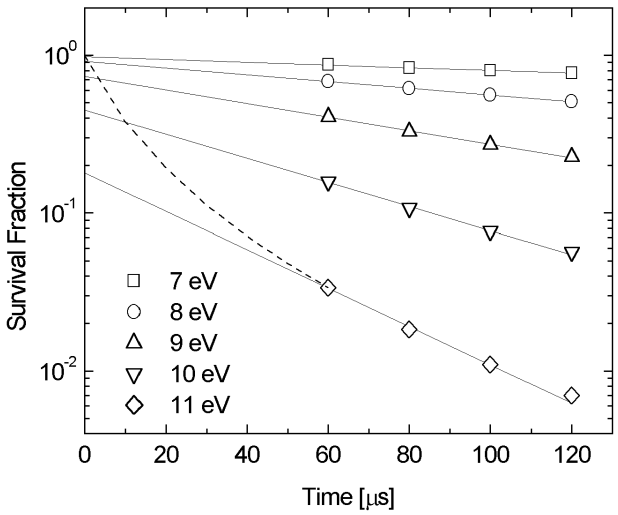

Figure 8. Simulation of the experiments in [26] and [32]. An electron was attached to C_{60} molecules emerging from an oven at 775 K, at the electron energies given in the figure, and the current of surviving ions was measured after delay times between 60 and 120 μs. The points give our results for the surviving fraction, based on equations (16) and (20), with the first-order expression in equation (18) and with the parameters discussed in the text. The solid curves are exponential fits to the points in the time range of the measurements, and the dashed curve shows how the calculated survival fraction varies from 0 to 60 μs for the highest electron energy.

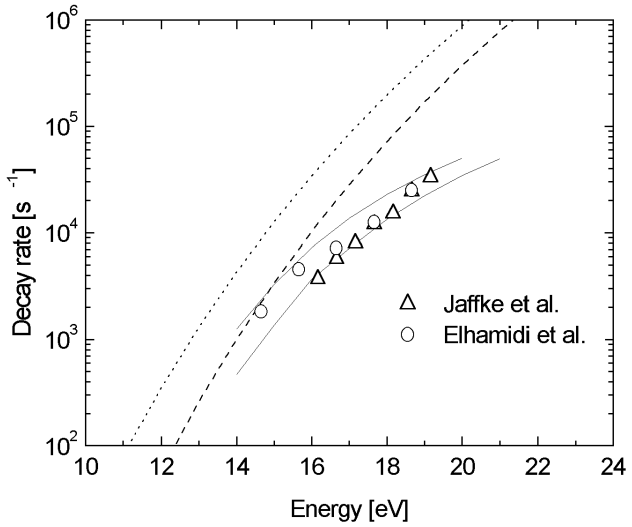

Figure 9. Decay rates against average excitation energy for C_{60}^-, determined as illustrated by the exponential fits in figure 8. The points are from [26,32]. The two solid curves are from calculations, with pre-exponential factors corresponding to attachment cross sections of 20 and 60 Å^2 (upper curve). The latter value was used for calculation of the decay rate without depletion, for a canonical energy distribution (dotted) and for a delta function (dashed).

the results to be in rough agreement with the detailed-balance requirement [27]. However, on closer inspection there seems to be a significant discrepancy [95]: the pre-exponential factor in an Arrhenius representation of the decay constant appears to be lower by orders of magnitude

than the prediction in equation (6). We shall show that this discrepancy results from an analysis which does not include the width of the energy distributions.

In these experiments, the C_{60} molecules were produced in an oven at temperatures near 800 K. There is conflicting information on the oven temperature in the various accounts of one experiment [26, 27] and even within the same paper on another [32], but most likely the gas pressures and hence the temperatures were similar in the different experiments on the same molecule. We have chosen $T = 775$ K for the analysis of C_{60}. The relation between excitation energy and temperature may be obtained from the calculated spectrum of vibrations [55, 61], and in the range 1000–2000 K the linear relation

$$\bar{E}[\mathrm{eV}] = 7.4 + 0.0138(T[\mathrm{K}] - 1000), \tag{34}$$

is a good approximation. It corresponds to a heat capacity $C \simeq 160k_B$ and we need not distinguish between canonical and microcanonical values since the difference is less than 1%. With a small correction to the expression in equation (34) below 1000 K [61], we obtain an average excitation energy of 4.8 eV for molecules exiting the oven. The canonical energy distribution is nearly Gaussian and the rms width $(Ck_B)^{1/2}T$ [50] equals 0.85 eV. An electron from a crossed beam was attached and the final average energy is obtained by addition of the electron energy and the electron affinity of $E_b = 2.67$ eV [97]. We have assumed that the spread in electron energy is small compared with the thermal width.

The mass spectrometers used in the experiments allowed a determination of the ion current as a function of flight time in the range 60–120 μs. We have calculated the corresponding surviving fraction from equation (20), with a decay constant obtained from equations (16) and (18) with only the first-order correction to the temperature, and with the linear relation in equation (34) between the microcanonical variables E and T_m. The pre-exponential frequency calculated from equation (6) is $\nu = 3.0 \times 10^6 (T_d\ [\mathrm{K}])^2\ \mathrm{s}^{-1}$ for an attachment cross section of 60 Å^2 and with the sixfold degeneracy of the LUMO level of C_{60} included in ν. The resulting survival probabilities are shown in figure 8 for electron energies used in the experiments. The curves through the points are exponential fits in the range 60–120 μs, just as in the experiments, and the graphs are very similar to the plots of ion current versus delay time in figure 4 of [26] and figure 5 of [32]. For the highest electron energy, we also show the initial part of the survival curve, which was out of reach in the experiments. The decay rate, which determines the slope of the curve, decreases strongly in this region owing to depletion of the high-energy part of the distribution. This feature was not included in the original analysis of the experiments. The exponential fits were extrapolated to zero time delay and the decrease of the ion current at $t = 0$ as a function of excitation energy was interpreted as a decrease of the capture cross section for electron energies above 7 eV.

The calculated emission rate as a function of excitation energy is compared with the measured values in figure 9. The two solid curves correspond to attachment cross sections of 20 and 60 Å^2, and the experimental points fall between these lines. We have also included two curves representing the decay rate without depletion, both calculated for the same average energy and with $\sigma_c = 60$ Å^2. The dashed curve corresponds to decay of an ensemble of ions with a very narrow energy distribution, while the dotted curve illustrates electron emission in a thermal equilibrium, where the canonical energy distribution is maintained during the decay. The rate constant is then given by equation (16) with T_e equal to the canonical temperature. This was the formula used in the original analysis of the experiments. We conclude that for C_{60} the measurements of attachment cross sections and of lifetimes for electron emission fulfil the detailed-balance symmetry within the experimental uncertainty.

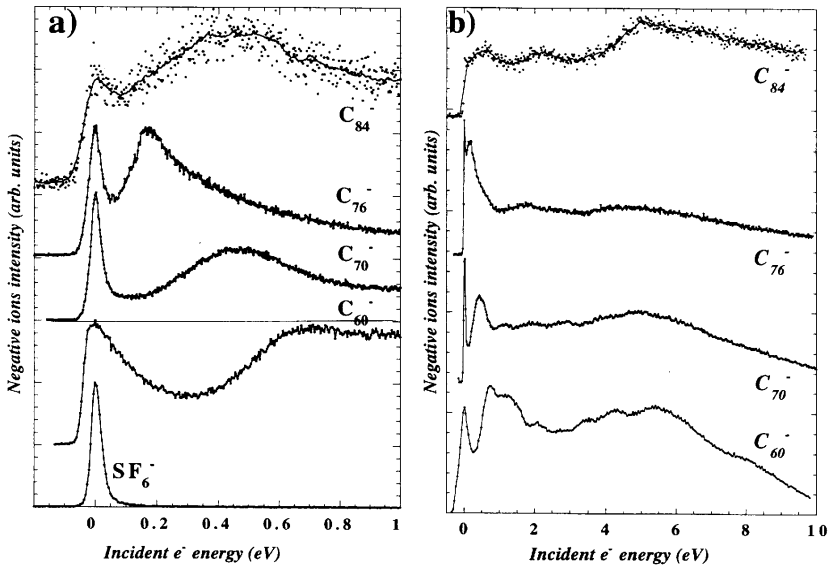

Figure 10. Relative values of attachment cross sections for C_{60}, C_{70}, C_{76} and C_{84} measured with a molecular beam from an oven and a crossing electron beam (from [34]). To the left (*a*) is given an expanded view of the results for energies below 1 eV. The results for attachment to SF_6 molecules calibrate the energy scale since there is a strong resonance at zero energy for this molecule.

8.3. Delayed electron emission after attachment to other fullerenes

Recently, this type of measurement has been extended to other fullerene ions, C_{70}^-, C_{76}^- and C_{84}^- [34]. Measured relative yields of anions formed by electron attachment are shown in figure 10, with an expanded view of the low-energy region to the left. The comparison with resonance attachment to SF_6 molecules near zero energy again shows that the fullerenes can capture electrons with very low energy. There is considerable structure in the spectra at low energies, but they become smooth above a few eV. It is likely that the decrease of the yields towards 10 eV for the lighter fullerenes is caused by electron re-emission before detection of the ions and that hence the attachment cross section is fairly constant at the higher energies in figure 10(*b*). The values are probably close to the geometrical cross sections as previous measurements for C_{60} have indicated, and the average magnitude at the lowest energies is similar, except for C_{76} where it appears to be about twice as large.

The results of the lifetime measurements are in figure 11 plotted against the average excitation energy of the emitting anions. The initial thermal energy was evaluated at temperatures of 775 and 800 K for C_{60} and C_{70} and 925 K for C_{76} and C_{84} [34], and the electron affinities were chosen as 2.67 eV for C_{60} and C_{70}, 3 eV for C_{76} and 3.15 eV for C_{84} [92]. The emission rates were calculated as for C_{60}^- (figure 9), with a heat capacity scaled by the number of atoms and with a pre-exponential frequency ν in equation (5) corresponding to a capture cross section proportional to N and for $N = 60$ equal to the mean of the two cross sections used in figure 9, $\sigma_c = 40$ Å^2. The degeneracy of the LUMO level occupied by the additional electron in the anions appears to be similar in C_{60} and C_{70} [98, 99] but should perhaps be reduced in the less symmetric molecules, where also the presence of several isomers is a complication [100]. For simplicity we have used the same sixfold degeneracy for all molecules.

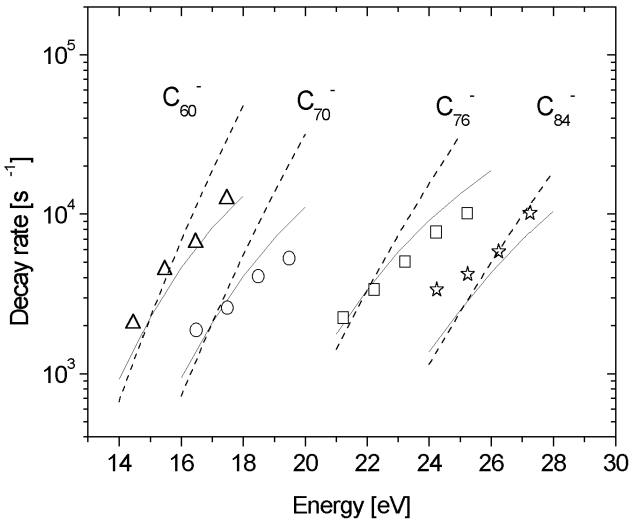

Figure 11. Analysis of the measurements in [34] of the decay rate as a function of excitation energy for fullerene anions. The dashed curves represent the rate constant in equation (16) with the parameters given in the text, whereas the full curves were calculated in analogy with the full curves in figure 9, with capture cross sections scaled from the value $\sigma_c = 40$ Å^2 for C_{60}, as explained in the text.

As seen in figure 11, the calculations are in reasonable, albeit not perfect, agreement with the measurements. As before, the decay rate for a very narrow energy distribution (dashed curves) has a much steeper energy dependence than obtained with the finite width of the distributions. The relative displacements of the curves along the energy axis are roughly in agreement with the variations of the heat capacity, with a correction for the differences in electron affinity, and this is strong evidence for a full redistribution of the excitation energy over the degrees of freedom of the molecules before re-emission of the captured electron. For C_{84}^- the decay rates are somewhat above the calculations, and this may indicate a lower degeneracy of the LUMO level. In the data for C_{76}^- there is no sign of such a reduced degeneracy or of the apparently very high capture cross section, which should also increase the pre-exponential frequency. However, the attachment yields could be different at the much higher temperatures where the emission takes place. We conclude that the measurements for the other fullerene anions give further support to the interpretation of delayed electron emission as thermionic emission, although the uncertainties are somewhat larger than for C_{60}^-.

8.4. Electron emission after laser excitation of C_{60}^-

We finally mention a very recent experiment analogous to those on small Nb clusters discussed in section 7 [62]. C_{60}^- ions were injected from a cold source into a small storage ring, where they were excited by a pulse of higher-harmonic radiation from a Nd:YAG laser. Electron emission was monitored as a function of time after the excitation, and the results obtained with second-harmonic radiation are shown in figure 12. The early part of the decay corresponds to a lifetime of 0.35 ms, and from observation of the same lifetime with excitation by third- and fourth-harmonic radiation it was concluded that six second-harmonic photons have been absorbed (about 14 eV). Higher photon numbers contribute only to the first one or two points, but at the longer times the observed decay curve is dominated by absorption of only five

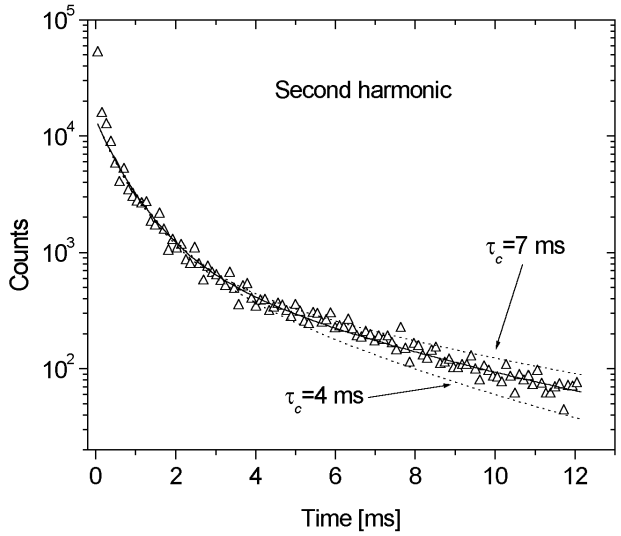

Figure 12. Decay by electron emission of C_{60}^- ions, produced by a cold source (electrospray) and stored in the small storage ring ELISA (from [62]). The time equals the delay after excitation of the ions by a pulse of second-harmonic radiation from a Nd:YAG laser, and the solid curve is a fit including absorption of five or six photons. The lifetimes have been obtained from equation (16), with ν given by equation (6) with $\sigma_c = 42$ Å^2. Radiative cooling consistent with [61] has been included, and the dotted curves show the sensitivity to the cooling time τ_c introduced in [62].

photons. At this excitation energy the decay is strongly influenced by radiative cooling. It is shown in [62] that all the measurements can be fitted with decay rates calculated from equation (16) with an attachment cross section $\sigma_c = 42$ Å^2 in equation (6) and with inclusion of a radiative cooling rate consistent with the measurement in [61]. This confirms the result of our analysis in section 8.2.

9. Conclusions

We have discussed the statistical description of delayed electron emission from clusters and its application to the analysis of experiments. We have argued that transition state theory is not a suitable framework and have instead applied a more general formalism based on detailed balance, which can also be applied to derive the Richardson–Dushman formula for thermionic emission from a macroscopic surface. In this formula, the level of excitation of the material is characterized by a thermodynamic temperature, but for an isolated cluster one must distinguish between several temperatures. We have argued that the appropriate concept is the microcanonical temperature, defined in terms of the logarithmic derivative of the level density. For thermionic emission, the energy distribution of emitted electrons is governed by the microcanonical temperature after emission, while the temperature entering an Arrhenius expression for the decay rate is close to the average of the microcanonical temperatures before and after emission. The differences are due to the finite heat capacity of the system, and our description is closely related to Klots' finite-heat-bath theory. However, Klots does not introduce the concept of a microcanonical temperature.

Two examples have been analysed in detail. For measurements of electron emission from small Nb clusters, our first analysis agrees in general with the original interpretation of the data: the energy barriers are somewhat lower than the ionization potentials and the pre-exponential

frequencies are very low, $\nu \sim 10^{11}$ s^{-1}. We have examined two modifications, an increase of the heat capacity beyond the Dulong–Petit value, as for bulk Nb, and competition by radiative decay. The combined effect is to bring the barrier into agreement with the ionization potential and to increase ν by two orders of magnitude. The value of ν is still lower than expected, but since theoretical estimates include a large uncertainty related to the sticking probability in electron attachment, the experiments may be consistent with the hypothesis of an internal statistical equilibrium.

Our second and most important example is electron emission from fullerene anions. In this case, both the heat capacity and the radiative cooling are known quite accurately. Electron attachment to neutral fullerenes and electron emission from the anions have been measured by several groups, and this allows a calculation of emission rates based on detailed balance and measured capture cross sections. We have demonstrated that the data are consistent with the calculated rates and this lends strong support to the interpretation of delayed electron emission from buckminsterfullerene anions as thermionic emission. The main reason for the opposite conclusion in earlier discussions appears to be that the finite width of the internal-energy distributions of the anions had not been taken into account in the analysis of experiments. A very recent experiment on electron emission after laser excitation of cold C_{60}^- ions has confirmed these conclusions.

Acknowledgments

This work was supported by the Danish National Research Foundation through the Aarhus Centre for Atomic Physics and by the EU Research Training Network, contract HPRN-CT2000-00026.

Appendix

Experiments on delayed electron emission have often been analysed with a formalism based on transition state theory. To illustrate the connection between such a picture and the Weisskopf formalism in section 2.1 we evaluate the emission rate in analogy to the description of neutron emission from a heavy nucleus in [44, section III]. The following calculation is also closely analogous to the derivation of our equation (2). The electron is now treated as a classical particle, and its interaction with the cluster is assumed to vanish outside the cluster radius r. In a transition state of the system, an electron with energy ϵ is found within a spherical shell of thickness Δl outside the surface $4\pi r^2$ of the daughter cluster with level density ρ_d. We consider a microcanonical ensemble of clusters, all having excitation energy between E and $E + \mathrm{d}E$, with one cluster in each quantum state, including the two directions of the electron spin. The number of transition states for which the electron momentum lies in the range from p to $p + \mathrm{d}p$ and within the solid angle $\mathrm{d}\Omega$ is given by

$$\mathrm{d}n = (2 \cdot 4\pi r^2 \Delta l \cdot p^2 \,\mathrm{d}p \,\mathrm{d}\,\Omega / h^3)\rho_d(E - E_b - \epsilon)\,\mathrm{d}E. \tag{A.1}$$

To calculate the rate constant for emission, we first multiply $\mathrm{d}n$ by the spatial density of an electron in the transition state, $(4\pi r^2 \Delta l)^{-1}$, and by the product of the surface area and the normal velocity $v\cos\theta = (\mathrm{d}\epsilon/\mathrm{d}p)\cos\theta$. Then we integrate over directions and over ϵ and find for the number of electron emission processes per unit time in the ensemble,

$$\mathrm{d}E(2 \cdot 4\pi r^2 \cdot 2\pi m/h^3)\int_0^{E-E_b} \rho_d(E - E_b - \epsilon)\,\epsilon\,\mathrm{d}\epsilon. \tag{A.2}$$

The rate constant is finally obtained through division by the total number of parent systems, $\rho_p(E)\,\mathrm{d}E$, and this leads to

$$k(E) = \frac{(2 \cdot 4\pi r^2 \cdot 2\pi m/h^2) \int_0^{E-E_b} \rho_d(E - E_b - \epsilon)\epsilon \,\mathrm{d}\epsilon}{h\rho_p(E)}. \tag{A.3}$$

We can compare this formula with the expression obtained from transition state theory,

$$k(E) = \frac{\int_0^{E-E_b} \rho^+(E')\,\mathrm{d}E'}{h\rho_p(E)}, \tag{A.4}$$

where ρ^+ denotes the level density at the transition state. The two expressions for $k(E)$ become identical if we choose $\rho^+(E')$ as the daughter level density $\rho_d(E')$ multiplied by the number of quantum states for energies below $E - E_b - E'$ in the electron motion perpendicular to the emission direction.

As mentioned in the introduction, there are several unrealistic features in this transition state calculation: the electrons are treated as classical particles, their interaction with the cluster is assumed to vanish outside the cluster radius, and in the equilibrium ensemble all electrons moving away from the cluster are assumed to originate from inside, i.e. the contribution from incoming electrons which are reflected is ignored. In the Weisskopf formalism, these assumptions are avoided. There is, however, a very simple connection between the two descriptions. If we replace the surface area $4\pi r^2$ in equation (A.3) by four times the capture cross section $\sigma_c(\epsilon)$, the formula in equation (2) is recovered. For this equivalence, it is important that the number of quantum states in the transverse motion of the emitted electron be included in the level density ρ^+ in equation (A.4), and in applications this factor has often been omitted [8]. However, in the case of electron emission from a neutral cluster, where the capture cross section should scale as $\sigma_c \propto \epsilon^{-1}$ according to equation (10), equation (A.4) with omission of the electron phase space factor happens to agree with equation (A.3) with πr^2 replaced by σ_c, to within a constant factor which is unimportant when the formula is used in a fitting procedure as in [8].

References

[1] Campbell E E B and Levine R D 2000 *Ann. Rev. Phys. Chem.* **51** 65
[2] Klein-Weile J H, Simon P and Rubahn H-G 1998 *Phys. Rev. Lett.* **80** 45
[3] Simon M, Träger F, Assion A, Lang B, Voll S and Gerber G 1998 *Chem. Phys. Lett.* **296** 579
[4] Schlipper R, Kusche R, von Issendorff B and Haberland H 1998 *Phys. Rev. Lett.* **80** 1194
[5] Weber J M, Hansen K, Ruf M-W and Hotop H 1998 *Chem. Phys.* **239** 271
[6] Campbell E E B, Hansen K, Hoffmann K, Korn G, Tchaplyguine M, Wittmann M and Hertel I V 2000 *Phys. Rev. Lett.* **84** 2128
[7] Schlipper R, Kusche R, von Issendorff B and Haberland H 2001 *Appl. Phys.* A **72** 2554
[8] Collings B A, Amrein A H, Rayner D M and Hackett P A 1993 *J. Chem. Phys.* **99** 4174
[9] Yeretzian C, Hansen K and Whetten R L 1993 *Science* **260** 652
[10] O'Neal D and Simons J 1989 *J. Phys. Chem.* **93** 58
[11] Kooi S E and Castleman A W Jr 1998 *J. Chem. Phys.* **108** 8864
[12] Herring C and Nichols M H 1949 *Rev. Mod. Phys.* **21** 185
[13] Ganteför G, Eberhardt W, Weidele H, Kreisle D and Recknagel E 1996 *Phys. Rev. Lett.* **77** 4524
[14] Amrein A, Simpson R and Hackett P 1991 *J. Chem. Phys.* **95** 1781
[15] Leisner T, Athanassenas K, Kreisle D, Recknagel E and Echt O 1993 *J. Chem. Phys.* **99** 9670
[16] Weidele H, Kreisle D, Recknagel E, Schulze Icking-Konert G, Handschuh H, Ganteför G and Eberhardt W 1995 *Chem. Phys. Lett.* **237** 425
[17] Pinaré J C, Baguenard B, Bordas C and Broyer M 1998 *Phys. Rev. Lett.* **81** 2225
[18] Weidele H, Kreisle D, Recknagel E, Becker St, Kluge H-J, Lindinger M, Schweikhard L, Walther C and Ziegler J 1999 *J. Chem. Phys.* **110** 8754
[19] Baguenard B, Pinaré J C, Bordas C and Broyer M 2001 *Phys. Rev.* A **63** 023204

[20] Wang Lai-Sheng, Conceicao J, Jin Changming and Smalley R E 1991 *Chem. Phys. Lett.* **182** 5
[21] Campbell E E B, Ulmer G and Hertel I V 1991 *Phys. Rev. Lett.* **67** 1986
[22] Wurz P and Lykke K R 1991 *J. Chem. Phys.* **95** 7008
[23] Ding D, Compton R N, Haufler R E and Klots C E 1993 *J. Phys. Chem.* **97** 2500
[24] Lezius M, Scheier P and Märk T D 1993 *Chem. Phys. Lett.* **203** 232
[25] Smith D, Spanel P and Märk T D 1993 *Chem. Phys. Lett*. **213** 202
[26] Jaffke T, Illenberger E, Lezius M, Matejcik S, Smith D and Märk T D 1994 *Chem. Phys. Lett.* **226** 213
[27] Matejcik S, Märk T D, Spanel P, Smith D, Jaffke T and Illenberger E 1995 *J. Chem. Phys.* **102** 2516
[28] Huang J, Carman H S Jr and Compton R N 1995 *J. Phys. Chem.* **99** 1719
[29] Vostrikov A A, Dubov D Yu and Agarkov A A 1995 *Techn. Phys. Lett.* **21** 517
[30] Klots C E and Compton R N 1996 *Surf. Sci. Rev.* **3** 535
[31] Smith D and Spanel P 1996 *J. Phys. B: At. Mol. Opt. Phys.* **29** 5199
[32] Elhamidi O, Pommier J and Abouaf R 1997 *J. Phys. B: At. Mol. Opt. Phys.* **30** 4633
[33] von Helden G, Holleman I, van Roij A J A, Knippels G M H, van der Meer A F G and Meijer G 1998 *Phys. Rev. Lett.* **81** 1825
[34] Elhamidi O, Pommier J and Abouaf R 2001 *Int. J. Mass Spectrom.* **205** 17
[35] Sattler K, Mühlbach J, Echt O, Pfau P and Recknagel E 1981 *Phys. Rev. Lett.* **47** 160
[36] Knight W D, Clemenger K, de Heer W A, Saunders W A, Chou M Y and Cohen M L 1984 *Phys. Rev. Lett.* **52** 2141
[37] Clemenger K 1985 *Phys. Rev.* B **32** 1359
[38] Bjørnholm S 1990 *Contemp. Phys.* **31** 309
[39] Genzken O and Brack M 1991 *Phys. Rev. Lett.* **67** 3286
[40] Haberland H 1999 *Nucl. Phys.* A **649** 415
[41] de Heer W A, Selby K, Kresin V, Masui J, Vollmer M, Chatelain A and Knight W D 1987 *Phys. Rev. Lett.* **59** 1805
[42] Borggren J, Chowdhury P, Kebaïli N, Lundsberg-Nielsen L, Lützenkirchen K, Nielsen M B, Pedersen J and Rasmussen H D 1993 *Phys. Rev.* B **48** 17 507
[43] Bohr N 1936 *Nature* **137** 344
[44] Bohr N and Wheeler J A 1939 *Phys. Rev.* **56** 426
[45] Wigner E 1938 *Trans. Faraday Soc.* **34** 29
[46] Weisskopf V 1937 *Phys. Rev.* **52** 295
[47] Klots C E 1991 *Chem. Phys. Lett.* **186** 73
[48] Klots C E 1989 *J. Chem. Phys.* **90** 4470
[49] Klots C E 1990 *J. Chem. Phys.* **93** 2513
[50] Andersen J U, Bonderup E and Hansen K 2001 *J. Chem. Phys.* **114** 6518
[51] Hansen K, Andersen J U, Hvelplund P, Møller S P, Pedersen U V and Petrunin V V 2001 *Phys. Rev. Lett.* **87** 123401
[52] Frenzel U, Kalmbach U, Kreisle D and Recknagel E 1996 *Surf. Rev. Lett.* **3** 505
[53] Frenzel U, Hammer U, Westje H and Kreisle D 1997 *Z. Phys.* D **40** 108
[54] Mitzner R and Campbell E E B 1995 *J. Chem. Phys.* **103** 2445
[55] Andersen J U, Brink C, Hvelplund P, Larsson M O, Bech Nielsen B and Shen H 1996 *Phys. Rev. Lett.* **77** 3991
[56] Andersen J U, Brink C, Hvelplund P, Larsson M O and Shen H 1997 *Z. Phys.* D **40** 365
[57] Bohren C F and Huffman D R 1983 *Absorption and Scattering of Light by Small Particles* (New York: Wiley)
[58] Halperin W P 1986 *Rev. Mod. Phys.* **58** 533
[59] Kreibig U and Vollmer M 1995 *Optical Properties of Metal Clusters* (Berlin: Springer)
[60] Andersen J U and Bonderup E 2000 *Eur. Phys. J.* D **11** 413
[61] Andersen J U, Gottrup C, Hansen K, Hvelplund P and Larsson M O 2001 *Eur. Phys. J.* D **17** 189
[62] Andersen J U, Hvelplund P, Nielsen S B, Pedersen U V and Tomita S 2002 *Phys. Rev.* A at press
[63] Marcus R A 1966 *J. Chem. Phys.* **45** 2138
[64] Klots C E 1971 *J. Phys. Chem.* **75** 1526
[65] Blatt J M and Weisskopf V F 1952 *Theoretical Nuclear Physics* (New York: Wiley)
[66] Gilbert R G and Smith S C 1990 *Theory of Unimolecular and Recombination Reactions* (Oxford: Blackwell) ch 3
[67] Bertsch G F, Oberhofer N and Stringari S 1991 *Z. Phys.* D **20** 123
[68] Fröbrich P 1995 *Phys. Lett.* A **202** 99
[69] Gross D H E and Hervieux P A 1995 *Z. Phys.* D **35** 27
[70] Frauendorf S 1995 *Z. Phys.* D **35** 191
[71] Hansen K 1999 *Phil. Mag.* B **79** 1413

[72] Kresin V V and Guet C 1999 *Phil. Mag.* B **79** 1401
[73] Kasperovich V, Wong K, Tikhonov G and Kresin V V 2000 *Phys. Rev. Lett.* **85** 2729
[74] Vogt E and Wannier G H 1954 *Phys. Rev.* **95** 1190
[75] Kasperovich V, Tikhonov G, Wong K, Brockhaus P and Kresin V V 1999 *Phys. Rev.* A **60** 3071
[76] Kasperovich V, Tikhonov G, Wong K and Kresin V V 2000 *Phys. Rev.* A **62** 063201
[77] Buckman S J and Clark C W 1994 *Rev. Mod. Phys.* **66** 539
[78] Finch C D, Popple R A, Nordlander P and Dunning F B 1995 *Chem. Phys. Lett.* **244** 345
[79] Weber J M, Ruf M-W and Hotop H 1996 *Z. Phys.* D **37** 351
[80] Bates D R 1994 *Adv. At. Mol. Phys.* **34** 427
[81] Ingolfsson O, Weik F and Illenberger E 1996 *Int. J. Mass. Spectrom. Ion Process.* **155** 1
[82] Mitchell J B A and Rebrion-Rowe C 1997 *Int. Rev. Phys. Chem.* **16** 201
[83] Lindhard J 1986 *The Lesson of Quantum Theory* ed J de Boer, E Dal and O Ulfbeck (Amsterdam: North-Holland) p 99
[84] Weaver J H, Lynch D W and Olson C G 1973 *Phys. Rev.* B **7** 4311
[85] Hansen K and Campbell E E B 1996 *J. Chem. Phys.* **104** 5012
[86] Tomita S, Andersen J U, Gottrup C, Hvelplund P and Pedersen U V 2001 *Phys. Rev. Lett.* **87** 073401
[87] Pettiette C L, Yang S H, Craycraft M J, Conceicao J, Laaksonen R T, Chesnovsky O and Smalley R E 1988 *J. Chem. Phys.* **88** 5377
[88] Zhang Y and Stuke M 1993 *Phys. Rev. Lett.* **70** 3231
[89] Lykke K R 1995 *Phys. Rev. Lett.* **75** 1234
[90] Touloukian Y S and Buyco E H 1970 *Thermophysical Properties of Matter* vol 4 (New York: IFI) p 153
[91] *Handbook of Chemistry and Physics* 1991–1992 72nd edn (Boston: CRC Press)
[92] Boltalina O V, Dashkova E V and Sidorov L N 1996 *Chem. Phys. Lett.* **256** 253
[93] Tosatti E and Manini N 1994 *Chem. Phys. Lett.* **223** 61
[94] Lucchese R R, Gianturco F A and Sanna N 1999 *Chem. Phys. Lett.* **305** 413
[95] Campbell E E B and Levine R D 1999 *Comments Mod. Phys.* D **1** 155
[96] Honea E C, Homer M L, Persson J L and Whetten R L 1990 *Chem. Phys. Lett.* **171** 147
[97] Brink C, Andersen L H, Hvelplund P, Mathur D and Voldstad J O 1995 *Chem. Phys. Lett.* **233** 52
[98] Saito S and Oshiyama A 1991 *Phys. Rev.* B **44** 11 532
[99] Lawson D R, Feldheim D L, Foss C A, Dorhout P K, Elliott C M, Martin C R and Parkinson B 1992 *J. Phys. Chem.* **96** 7175
[100] Saito S, Sawada S and Hamada N 1992 *Phys. Rev.* B **45** 13 845